MRI-Visible Perivascular Spaces in the Centrum Semiovale Are Associated with Brain Amyloid Deposition in Patients with Alzheimer Disease–Related Cognitive Impairment

H.J. Kim, H. Cho, M. Park, J.W. Kim, S.J. Ahn, C.H. Lyoo, S.H. Suh, and Y.H. Ryu

ABSTRACT

BACKGROUND AND PURPOSE: The association of perivascular spaces in the centrum semiovale with amyloid accumulation among patients with Alzheimer disease–related cognitive impairment is unknown. We evaluated this association in patients with Alzheimer disease–related cognitive impairment and β-amyloid deposition, assessed with [^{18}F] florbetaben PET/CT.

MATERIALS AND METHODS: MR imaging and [^{18}F] florbetaben PET/CT images of 144 patients with Alzheimer disease–related cognitive impairment were retrospectively evaluated. MR imaging–visible perivascular spaces were rated on a 4-point visual scale: a score of $\geq$3 or $<$3 indicated a high or low degree of MR imaging–visible perivascular spaces, respectively. Amyloid deposition was evaluated using the brain β-amyloid plaque load scoring system.

RESULTS: Compared with patients negative for β-amyloid, those positive for it were older and more likely to have lower cognitive function, a diagnosis of Alzheimer disease, white matter hyperintensity, the *Apolipoprotein E ε*4 allele, and a high degree of MR imaging–visible perivascular spaces in the centrum semiovale. Multivariable analysis, adjusted for age and *Apolipoprotein E* status, revealed that a high degree of MR imaging–visible perivascular spaces in the centrum semiovale was independently associated with β-amyloid positivity (odds ratio, 2.307; 95% CI, 1.036–5.136; $P = .041$).

CONCLUSIONS: A high degree of MR imaging–visible perivascular spaces in the centrum semiovale independently predicted β-amyloid positivity in patients with Alzheimer disease–related cognitive impairment. Thus, MR imaging–visible perivascular spaces in the centrum semiovale are associated with amyloid pathology of the brain and could be an indirect imaging marker of amyloid burden in patients with Alzheimer disease–related cognitive impairment.

ABBREVIATIONS: AD = Alzheimer disease; ADCI = AD-related cognitive impairment; APOE = Apolipoprotein E; BAPL = β-amyloid plaque load; [^{18}F] FBB = [^{18}F] florbetaben; MMSE = Mini-Mental State Examination; PVS = perivascular spaces; PVS-CS = perivascular spaces in the centrum semiovale; SUVr = standardized uptake value ratios; WMH = white matter hyperintensity

Accumulating evidence suggests that MR imaging–visible perivascular spaces (PVS) are not innocent lesions but may be a neuroimaging marker of cerebral small-vessel disease.[1-3] The

Indicates open access to non-subscribers at www.ajnr.org

Indicates article with online supplemental data.

http://dx.doi.org/10.3174/ajnr.A7155

perivascular space is a potential space filled with interstitial fluid surrounding penetrating vessels. It is involved in the drainage of interstitial fluid and solutes from the brain.[4] Therefore, several clinical conditions that reduce the clearance of solutes from the brain interstitial fluid such as aging, hypertension, and inflammation can result in MR imaging–visible PVS.[5] MR imaging–visible PVS are also associated with various diseases, such as traumatic brain injury, Parkinson disease, and dementia.[6-9] The location of MR imaging–visible PVS is an important factor to consider when predicting disease status because MR imaging–visible PVS in the basal ganglia may be associated with markers of arteriolosclerosis, whereas MR imaging–visible PVS in the centrum semiovale (PVS-CS) are linked to diseases involving amyloid pathology, such as Alzheimer disease (AD) and cerebral amyloid angiopathy.[10,11]

Many different studies on cerebral amyloid angiopathy have demonstrated a strong relationship between MR imaging–visible PVS-CS and cerebral amyloid angiopathy.[12-15] Some studies have
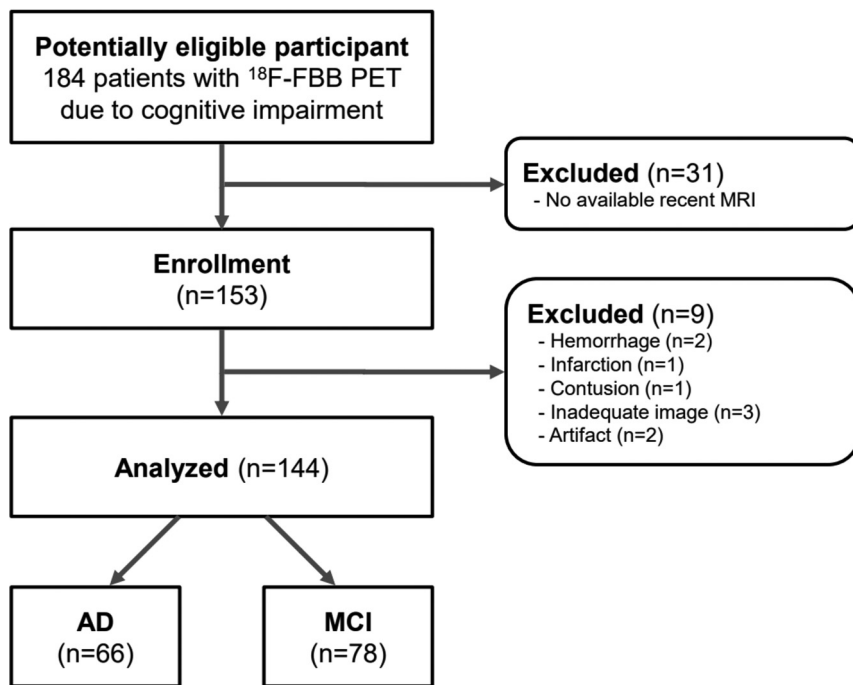
FIG 1. Patient-inclusion flowchart.

suggested that the dilation of PVS and failure in the drainage of interstitial fluid may result from deposition of β-amyloid in the cortical and leptomeningeal arteries.[16] Furthermore, evidence indicates that MR imaging–visible PVS-CS are associated with in vivo β-amyloid deposition in the brain, based on amyloid PET scanning,[14,17] which enables the visualization of brain amyloid deposition and measures the distribution and density of β-amyloid plaques.[18]

Failure in the perivascular clearance of β-amyloid may also be involved in the accumulation of β-amyloid in AD.[19] In patients with AD, MR imaging–visible PVS-CS may reflect impaired perivascular clearance of β-amyloid, and several studies have indicated a link between MR imaging–visible PVS and AD.[7,20] However, unlike evidence for the association between MR imaging–visible PVS-CS and cerebral amyloid angiopathy, scant evidence exists regarding the association between β-amyloid deposition and MR imaging–visible PVS in the population with dementia.

Several compounds labeled with radioisotopes have been developed to image amyloid deposition. In patients with cognitive impairment, PET scans using these tracers are widely used for diagnosis and follow-up.[21] Among the radiopharmaceuticals, [18F] florbetaben ([18F] FBB) is widely used for PET imaging to evaluate AD and other causes of dementia. [18F] FBB has a proper half-life and also allows high-resolution image acquisition, diagnostic capability, and quantification.[22] For these reasons, [18F] FBB is suitable for evaluating amyloid accumulation and its association with enlarged PVS in patients with dementia.

We hypothesized that MR imaging–visible PVS-CS would be associated with brain amyloid deposition in cognitively impaired patients, as it is in patients with cerebral amyloid angiopathy. We also evaluated the association using [18F] FBB, a PET radiotracer

that labels in vivo amyloid deposits, in patients with cognitive impairment.

MATERIALS AND METHODS
Participants
The need for written informed consent from patients was waived by the institutional review board of Gangnam Severance Hospital due to the retrospective nature of this study. Data were reviewed from 153 consecutive patients with cognitive impairment and clinical indications of AD-related cognitive impairment (ADCI). All patients underwent an [18F] FBB PET/CT and brain MR imaging within a 3-month interval from June 2017 to July 2019. Of the 153 patients with ADCI, we excluded 3 patients with inadequate image acquisition, 2 with image artifacts, 2 with intracranial hemorrhage, 1 with a large territorial infarction, and 1 with an old traumatic contusion. Therefore, 144 patients with ADCI were finally included in the analysis; among them, 66 patients had probable AD and 78 had mild cognitive impairment. Figure 1 shows the patient-inclusion flowchart. The criteria for probable AD, proposed by the National Institutes of Neurological and Disorders and Stroke and by the Alzheimer's Disease and Related Disorders Association[23], and the Petersen criteria,[24] were used for the clinical diagnosis of mild cognitive impairment.

Clinical Evaluation
We assessed all available patient information, such as basic demographic characteristics, other medical conditions (including a history of vascular risk factors), global cognitive assessment scores (eg, Clinical Dementia Rating Scale–Sum of Boxes score, Mini-Mental State Examination [MMSE] score, and a standardized neuropsychological battery called the Seoul Neuropsychological Screening Battery[25]), and Apolipoprotein E (APOE) ε4 genotyping. APOE genotyping was performed using the polymerase chain reaction. Individuals with at least 1 ε4 allele were classified as APOE ε4-positive.

MR Imaging Acquisition and Analysis
The MR imaging sequences were performed on a 3T scanner (Discovery MR750; GE Healthcare) with a 16-channel head coil. All patients underwent axial T2-weighted imaging, sagittal T1-weighted imaging, sagittal 3D-FLAIR, and axial 3D susceptibility-weighted angiography. Axial 2D T2-weighted images were acquired using the FSE sequence (TR/TE, 5320/102 ms; flip angle, 142°; section thickness, 4 mm; gap, 1 mm; FOV, 230 mm; matrix, 352 × 352). The actual TR/TE ranged from 5289/104 ms to 6028/97 ms due to the autoTR setting and specific absorption rate adjustment. Sagittal 3D T1-weighted images were obtained using the 3D fast-spoiled gradient echo sequence (TR/TE, 8.2/3.2 ms;

flip angle, 12°; section thickness, 1 mm; FOV, 240 mm; matrix, 256 × 256). Sagittal 3D-FLAIR images were obtained using the Cube sequence (GE Healthcare) (TR/TE, 6000/89 ms; TI, 1741 ms; section thickness, 1.2 mm; FOV, 260 mm; matrix, 256 × 224). Axial 3D susceptibility-weighted angiography images were obtained using the following parameters: TR/TE, 30.9/23.4 ms, 46.8 ms, and 70.2 ms; flip angle, 10°; section thickness, 2 mm; gap, 1 mm; FOV, 230 mm; and matrix, 320 × 224.

The PVS that were visible on MR imaging were assessed in line with the STandards for ReportIng Vascular changes on nEuroimaging recommendations.[26] Based on the axial T2-weighted MR images, MR imaging–visible PVS were rated in the basal ganglia and centrum semiovale using a validated 4-point visual rating scale: 0 = no PVS; 1 = ≤10 PVS; 2 = 11–20 PVS; 3 = 21–40 PVS; and 4 = ≥40 PVS.[12,27] The numbers refer to MR imaging–visible PVS on 1 side of the brain (ie, the side/section with the highest number of PVS after all relevant slices for each anatomic area were reviewed). We prespecified a dichotomized classification of MR imaging–visible perivascular space degree as "high degree" (ie, score of >2) or "low degree" (ie, score of ≤2). This definition is in line with the perivascular space burden used in previous studies and may be characteristic of amyloid pathology.[10,12]

White matter hyperintensities (WMHs) were defined as hyperintense white matter lesions on FLAIR images based on the STandards for ReportIng Vascular changes on nEuroimaging criteria and were graded using the Fazekas scale as "deep WMHs" (0 = absent; 1 = punctate; 2 = early confluent; 3 = confluent) or "periventricular WMHs" (0 = absent; 1 = caps or pencil-thin lining; 2 = smooth halo; 3 = irregular WMHs extending into the deep white matter).[26,28] The total Fazekas score was calculated by adding the periventricular and deep WMH scores. A score of >3 was considered WMH-positive.[28] Lacunes were defined as small lesions that were hypointense on T1-weighted images and hyperintense on T2-weighted images and had perilesional halos on FLAIR images.[26] Microbleeds were defined as small signal voids with associated blooming on susceptibility-weighted angiography images. The presence and number of lacunes and microbleeds were recorded as previously described.[26]

[¹⁸F] FBB PET Imaging Acquisition and Analysis

PET images were obtained using a Biograph mCT PET/CT scanner (Siemens). At 90 minutes after we injected 307.0 (SD, 32.2) MBq of [¹⁸F] FBB, PET data were acquired for 20 minutes. After we conducted attenuation and scatter correction, 3D-PET images were reconstructed in a 256 × 256 × 223 matrix with a voxel size of 1.591 × 1.591 × 1 mm using the ordered-subsets expectation maximization algorithm.

We defined the results of amyloid PET as "positive" when the visual assessment of [¹⁸F] FBB PET was scored as 2 or 3 on the brain β-amyloid plaque load (BAPL) scoring system based on the following: 1 = no tracer uptake, 2 = moderate tracer uptake, and 3 = pronounced tracer uptake.[29,30] The decision was based on visual assessment of each section on the axial plane. All scans were independently evaluated by 2 experienced nuclear medicine physicians, who reread all the studies while blinded to the original clinical reports and clinical information and reached a consensus.

In addition to the visual assessment, we also performed a semi-quantitative analysis to evaluate the cortical [¹⁸F] FBB retention in the PET/CT scans, as follows: Cortical regional standardized uptake value ratios (SUVr) were calculated for each patient in the 6 cortical ROIs (frontal, parietal, lateral temporal, precuneus, and anterior and posterior cingulate cortex regions). We used the cerebellar gray matter as the reference for SUVr calculation. The global composite florbetaben SUVr was calculated as the average of the SUVr value in each ROI.[29,31] On the basis of the SUVr analysis, an [¹⁸F] FBB PET was defined as positive (SUVr-positive) when the global composite florbetaben SUVr was >1.42, which was assessed against the histopathologic determination of β-amyloid in previous research.[32]

Statistical Analyses

Baseline characteristics were compared using the χ^2 or Fisher exact test for categoric variables, independent t tests for normally distributed continuous variables, and Mann–Whitney U tests for continuous variables that were not normally distributed. MR imaging–visible PVS in both the basal ganglia and centrum semiovale were considered categoric variables, respectively. They were subdivided by severity, as described previously. We explored the independent and pathophysiologically relevant predictors of brain amyloid deposition using logistic regression analyses based on our prespecified hypothesis and the results of univariable analyses (including variables with $P < .05$). Multivariable logistic regression analyses, including age, sex, APOE ε4 allele status, and high degree of MR imaging–visible PVS-CS were performed. The variables of interest in univariable analysis were included in the multivariable models using the enter method. Positive WMH was not included in the analysis because it was significantly associated with a high degree of MR imaging–visible PVS-CS ($P < .001$, based on the χ^2 test).

Random Forests Analysis

A total of 13 demographic and radiologic features, excluding WMH, were evaluated; these features included age, sex, hypertension, diabetes, hyperlipidemia, previous stroke, APOE ε4 allele, MR imaging–visible PVS in the basal ganglia, MR imaging–visible PVS-CS, lacunes, cortical superficial siderosis, lobar cerebral microbleeds, and deep cerebral microbleeds. The random forests model was trained with demographic and radiologic features to classify the amyloid positivity of the brain. The diagnostic ability of the random forests model using receiver operating characteristic analysis and the area under the receiver operating characteristic curve was calculated.

RESULTS

Study Participants

In this study, the total number of patients with ADCI was 144, comprising 67 patients with a BAPL score of one, 11 with a BAPL score of 2, and 66 with a BAPL score of 3. On the basis of the criteria of the BAPL scoring system, 67 patients were negative for β-amyloid deposition and 77 were positive for it. According to the SUVr analysis, 74 patients were negative for β-amyloid deposition and 70 patients were positive for it.

Among the 144 patients with ADCI, 3 had a PVS in the basal ganglia score of zero, 85 had a score of 1 in MR imaging–visible PVS in the basal ganglia, 32 had a score of two, 17 had a score of 3, and 7 had a score of 4 in terms of MR imaging–visible PVS in the basal ganglia. With regard to MR imaging–visible PVS-CS, 15 patients with ADCI had a score of one, 57 had a score of two, 56 had a score of 3, and 16 had a score of 4.

Comparison between Groups Positive and Negative for β-Amyloid

Age was significantly older in the patients positive for β-amyloid deposition than in patients negative for it (mean, 75.4 [SD,

7.6] years versus 71.3 [SD, 10.6] years; $P = .010$). The prevalence of the *APOE* ε4 allele ($P = .001$), WMH ($P = .013$), and AD ($P < .001$) was higher in patients with β-amyloid positivity than in patients with β-amyloid negativity. The patients with β-amyloid positivity had poorer cognitive function on the MMSE ($P < .001$), the Clinical Dementia Rating Scale ($P = .019$), and the Clinical Dementia Rating Scale–Sum of Boxes ($P < .001$) compared with patients with β-amyloid negativity (Table 1). A high degree of MR imaging–visible PVS-CS existed more frequently among patients with β-amyloid positivity than in patients with β-amyloid negativity (48/77 [62.3%] versus 24/67 [35.8%]; $P = .002$), whereas a high degree of MR imaging–visible PVS in the basal ganglia did not differ between groups positive and negative for β-amyloid (13/77 [16.9%] versus 11/67 [16.4%], $P = .297$) (Fig 2). Representative examples of PVS patterns with the corresponding [^{18}F] FBB PET findings are presented in Fig 3.

Quantitative SUVr Analysis

In the SUVr analysis, 43/70 (61.4%) with global composite SUVr positivity were classified as having a high degree of MR imaging–visible PVS-CS compared with 29/74 (39.2%) with SUVr negativity ($P = .008$), and the high degree of MR imaging–visible PVS in the basal ganglia did not differ between the SUVr-positive and SUVr-negative groups (12/70 [17.1%] versus 12/74 [16.2%], $P = .881$). The global composite SUVr was significantly higher in patients with a high degree of MR imaging–visible PVS-CS than in those with a low degree (1.52 versus 1.37, $P = .005$). In region-based analysis, all 6 ROIs showed statistically significant differences. The frontal (1.56 versus 1.37, $P = .004$), parietal (1.50 versus 1.38, $P = .009$), lateral temporal (1.31 versus 1.19, $P = .008$), precuneus (1.60 versus 1.43, $P = .008$), anterior cingulate (1.47 versus 1.36, $P = .044$), and posterior cingulate (1.69 versus 1.52, $P = .004$) regions showed higher SUVr values in the patients with a high degree of MR imaging–visible PVS-CS than in those a low degree, respectively.

MR Imaging–Visible PVS as a Predictor of β-Amyloid Positivity

In the univariate logistic regression analysis, a high degree of MR imaging–visible PVS-CS was a positive predictor of β-amyloid positivity based

Table 1: Baseline characteristics of the groups positive and negative for brain β-amyloid

	Amyloid-Negative	Amyloid-Positive	P Value
(No.) (%)	67 (46.5%)	77 (53.5%)	
Age (mean) (SD) (yr)	71.3 (10.6)	75.4 (7.6)	.010
Female sex (No.) (%)	44 (65.7%)	44 (57.1%)	.297
Hypertension (No.) (%)	25 (37.3%)	36 (46.8%)	.254
Diabetes mellitus (No.) (%)	10 (14.9%)	16 (20.8%)	.364
Hyperlipidemia (No.) (%)	9 (13.4%)	11 (14.3%)	.883
Previous stroke (No.) (%)	7 (10.4%)	4 (5.2%)	.238
APOE ε4 presence (No.) (%)	13 (19.4%)	33 (42.9%)	.001
High degree of MR imaging–visible PVS-CS (No.) (%)	24 (35.8%)	48 (62.3%)	.002
High degree of MR imaging–visible PVS-BG (No.) (%)	11 (16.4%)	13 (16.9%)	.297
AD (No.) (%)	19 (28.4%)	47 (61.0%)	<.001
MMSE (median) (IQR)	26 (23–28)	24 (20–26)	<.001
CDR (median) (IQR)	0.5 (0.5–0.5)	0.5 (0.5–1.0)	.019
CDR-SB (median) (IQR)	1.5 (0.5–3.0)	3.0 (1.5–4.5)	<.001
Lacunes (median) (IQR)	0 (0–0)	0 (0–0)	.778
cSS present (No.) (%)	1 (1.5%)	6 (7.8%)	.081
Lobar CMB (median) (IQR)	0 (0–0)	0 (0–1)	.117
Deep CMB (median) (IQR)	0 (0–0)	0 (0–0)	.160
WMH presence (No.) (%)	27 (40.3%)	47 (61.0%)	.013

Note:—IQR indicates interquartile range; PVS-BG, perivascular space in the basal ganglia; CMB, cerebral microbleed; CDR, Clinical Dementia Rating Scale; CDR-SB, Clinical Dementia Rating Scale–Sum of Boxes; cSS, cortical superficial siderosis.
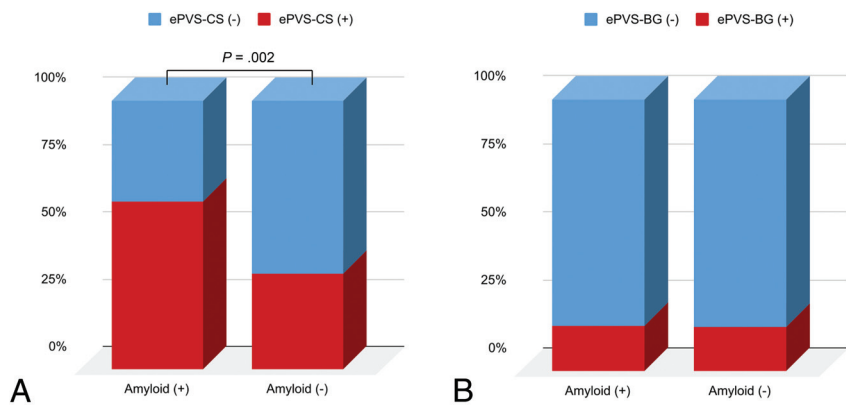

FIG 2. Comparisons of the presence of MR imaging–visible PVS-CS (*A*) and MR imaging–visible PVS in the basal ganglia (*B*) based on the β-amyloid status. The enlarged perivascular spaces in the centrum semiovale (ePVS-CS) were significantly higher in the patient group positive for β-amyloid than in the patient group negative for it, whereas the high degree of enlarged perivascular spaces in the basal ganglia (ePVS-BG) did not differ between the groups positive and negative for β-amyloid.

on the BAPL scoring system (OR, 2.966; 95% CI, 1.503–5.851; $P = .002$) (Table 2). After adjustment, a high degree of MR imaging–visible PVS-CS remained independently associated with β-amyloid PET positivity (OR, 2.307; 95% CI, 1.036–5.136; $P = .041$), as well as the presence of the $APOE\ \varepsilon4$ allele (OR, 4.583; 95% CI, 1.945–10.796; $P < .001$) and older age (OR, 1.050; 95% CI, 1.004–1.098; $P = .034$).

The random forests model with 13 variables showed an area under the curve of 0.985 (95% CI, 0.964–1.000) with an accuracy of 0.971 (95% CI, 0.931–1.000), sensitivity of 1.000 (95% CI, 1.000–

1.000), and specificity of 0.985 (95% CI, 0.964-1.000). We observed that MR imaging–visible PVS-CS ranked as the third most important variable after $APOE$ 4 and age (Online Supplemental Data).

Comparisons between Patients with High and Low Degrees of MR Imaging–Visible PVS-CS among Patients Positive for β-Amyloid

Among the 77 patients with ADCI with β-amyloid positivity, 70.8% of the patients with a high degree of MR imaging–visible PVS-CS had a higher proportion of positive WMHs (34/48), whereas 44.8% (13/29) of patients with a low degree of MR imaging–visible PVS-CS had positive WMHs ($P = .023$). The frequency of lobar microbleeds was also higher in patients with ADCI and β-amyloid positivity than among patients with ADCI and β-amyloid negativity ($P = .007$). Other parameters such as age, MMSE score, lacunes, deep microbleeds, sex, hypertension, diabetes mellitus, hyperlipidemia, previous stroke, the presence of an $APOE\ \varepsilon4$ allele, or final diagnosis were not significantly different between the patients with high and low degrees of MR imaging–visible PVS-CS (Online Supplemental Data).

Comparisons between Patients with High and Low Degrees of MR Imaging–Visible PVS-CS among Patients Negative for β-Amyloid

Among 67 patients with ADCI with β-amyloid negativity, the patients with a high degree of MR imaging–visible PVS-CS ($n = 24$) were older compared with patients with a low degree of MR imaging–visible PVS-CS ($n = 43$) (mean, 76.5 [SD, 9.8] years versus 68.3 [SD, 10.0] years; $P = .002$). Furthermore, the patients with a high degree of MR imaging–visible PVS-CS had lower MMSE scores compared with those with a low degree of MR imaging–visible PVS-CS (23.8 [SD, 4.0] versus 26.1 [SD, 3.7], $P = .018$). The patients with a high degree of MR imaging–visible PVS-CS compared with patients with a low degree of MR imaging–visible PVS-CS had a higher prevalence of hypertension (54.2% versus 27.9%, $P = .033$), positive WMHs (58.3% versus 30.2%, $P = .025$), final diagnosis of probable AD (45.8% versus
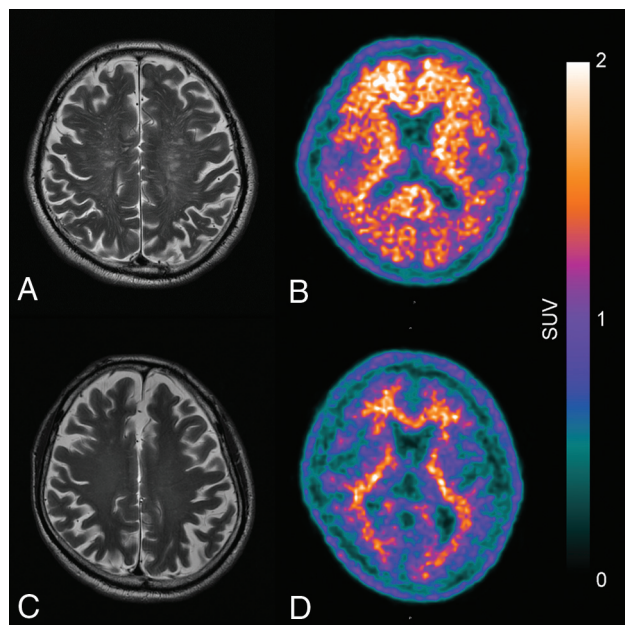

FIG 3. Examples of perivascular space patterns with the corresponding [^{18}F] FBB PET image. The axial T2-weighted MR imaging shows a high degree of MR imaging–visible PVS-CS (*A*), and the corresponding [^{18}F] FBB PET (*B*) shows pronounced β-amyloid deposition. Axial T2-weighted MR imaging shows a low degree of MR imaging–visible PVS-CS (*C*) and the [^{18}F] FBB PET scan (*D*) shows low β-amyloid deposition.

Table 2: Logistic regression analysis for the predictors of β-amyloid positivity

	Univariable		Multivariable	
	OR (95% CI)	P Value	OR (95% CI)	P Value
Age (yr)	1.051 (1.012–1.092)	.010	1.050 (1.004–1.098)	.034
Sex				
Female	Reference group			
Male	1.435 (0.729–2.823)	.296	1.561 (0.699–3.489)	.278
Hypertension (present)	1.475 (0.757–2.875)	.254		
Diabetes (present)	1.495 (0.627–3.564)	.364		
Hyperlipidemia (present)	1.074 (0.416–2.774)	.883		
Previous stroke (present)	0.470 (0.131–1.681)	.245		
$APOE\ \varepsilon4$ allele (present)	3.526 (1.630–7.627)	.001	4.583 (1.945–10.796)	<.001
High degree of MR imaging–visible PVS-CS (score, ≥3)	2.966 (1.503–5.851)	.002	2.307 (1.036–5.136)	.041
High degree of MR imaging–visible PVS-BG (score, ≥3)	1.034 (0.429–2.492)	.940		
WMH (present)	2.321 (1.188–4.533)	.014		
Lacunes (for 1 number higher)	0.937 (0.726–1.209)	.618		
cSS (present)	5.577 (0.654–47.565)	.116		
Lobar CMB (present)	1.100 (0.934–1.295)	.253		
Deep CMB (present)	0.688 (0.428–1.108)	.124		

Note:—CMB indicates cerebral microbleed; cSS, cortical superficial siderosis; MRI-visible PVS-BG, enlarged perivascular space in the basal ganglia; MRI-visible PVS-CS, enlarged perivascular space in the semi ovale.

18.6%, $P = .018$), and a higher number of lobar microbleeds (median, 0 [interquartile range, 0–0] versus 0 [interquartile range, 0–1]; $P = .007$). Other results are presented in the Online Supplemental Data.

DISCUSSION

In this retrospective study, we hypothesized that MR imaging–visible PVS-CS would be associated with brain amyloid deposition in patients with ADCI. We found that a high degree of MR imaging–visible PVS-CS were independently associated with β-amyloid accumulation, as assessed by [18F] FBB PET scanning, even after adjusting for previously known clinical risk factors. Our findings support the evidence that MR imaging–visible PVS-CS are associated with the amyloid pathology of the brain and could be an indirect imaging marker of amyloid burden in the brains of patients with ADCI.

PVS become visible on MR imaging when enlarged and can be detected in individuals of all ages; however, MR imaging–visible PVS are more frequently found with aging.[17,33] A recent meta-analysis, including a total of 8395 individuals, showed strong evidence for the association with age and MR imaging–visible PVS in the basal ganglia, as well as in the centrum semiovale.[33] On the other hand, a greater number of MR imaging–visible PVS can also be associated with various pathologic conditions. Accumulating evidence shows that MR imaging–visible PVS-CS, in particular, are associated with amyloid-associated pathology; several different studies have demonstrated an association with the presence of AD and MR imaging–visible PVS-CS,[7,20,34] though the mechanisms of MR imaging–visible PVS-CS remain poorly understood. However, our observation suggests a potential pathophysiologic link between AD and MR imaging–visible PVS, in that progressive β-amyloid deposition in the vascular wall or brain cortex may interfere with the perivascular drainage of interstitial fluid and ultimately cause retrograde perivascular space dilation in the white matter.[35] Consequently, the visibility of MR imaging–visible PVS is increased on MR imaging and appears as spaces with a signal intensity similar to that of CSF, resulting in a high burden of MR imaging–visible PVS.[8] Consistent with this hypothesis, a postmortem study of AD demonstrated that the degree of white matter PVS on histopathologic examination was positively correlated with cortical β-amyloid deposition,[16] which is in line with our observation. Therefore, visible PVS on brain MR imaging may result from abnormal amyloid accumulation in the cortex and cortical/leptomeningeal vessels.

Recently, advances in bioimaging and radiochemistry have enabled the in vivo imaging of β-amyloid deposits of AD, and this could be beneficial in aiding the early diagnosis of AD, compared with the use of clinical symptoms alone.[36-38] Furthermore, the use of biomarkers may also identify individuals who could benefit from disease-modifying therapies in AD. On the basis of our results, MR imaging–visible PVS alone cannot be an alternative to an amyloid PET scan; however, MR imaging–visible PVS-CS could be a useful indirect marker of amyloid deposition and may also be helpful in determining which patients with cognitive impairment are most likely to benefit from a biomarker test. These approaches may decrease the unnecessary patient burden and the costs of clinical practice and clinical trials.

To date, unlike the evidence for the cerebral amyloid angiopathy population,[14,17] scarce evidence exists regarding the association between AD and the in vivo amyloid burden, as assessed with PET. A previous study, with results conflicting with ours, showed that there was no association between MR imaging–visible PVS and amyloid burden in patients with dementia.[7] However, several considerable differences were found in terms of the study methodology, which may lead to different study outcomes.[7] First, the aforementioned study included a population with AD and vascular cognitive impairment, unlike our ADCI population. Because they included a large vascular dementia population, the heterogeneity of the diagnosis and probable higher severity of small-vessel disease in the population may lead to different results between the 2 studies. The amyloid-negative group in the aforementioned study had an inevitably higher WMH volume load, which may result in the misdiagnosis of MR imaging–visible PVS and ultimately interfere with the evaluation of the association between MR imaging–visible PVS and amyloid positivity. Furthermore, the different cutoff values for MR imaging–visible PVS scores may also lead to different study results. Those investigators considered score 2 (11–20 PVS) as a moderate pathologic condition, whereas we considered score 2 as a low degree of MR imaging–visible PVS. We believe that due to the wider area of the centrum semiovale compared with the basal ganglia and consequent higher number of PVS in the centrum semiovale than in basal ganglia, when one focuses on PVS in the centrum semiovale, score 2 should be considered a lower degree of PVS as it has been in other studies.[10,12]

Most interesting, we found that the group negative for β-amyloid had many different clinical variables that may be associated with a high degree of MR imaging–visible PVS-CS, such as aging, hypertension, and lower cognitive function in addition to AD pathology, lobar microbleeds, and the presence of WMHs. Therefore, we hypothesized that in patients with ADCI with lower amyloid burden, the presence of an MR imaging–visible PVS may have multifactorial causes, such as arterial stiffness and atrophy,[39,40] whereas in patients with ADCI and a high amyloid burden, MR imaging–visible PVS are primarily caused by amyloid accumulation. However, this hypothesis needs further validation.

In multivariate analysis, MR imaging–visible PVS-CS, APOE ε4 allele presence, and older age were significantly related to β-amyloid PET positivity, as analyzed by the BAPL scoring system. The visual assessment of [18F] FBB PET images has achieved high diagnostic accuracy, with the neuropathology assessments offering good reliability and efficacy.[41,42] We believe that using the BAPL scoring system to evaluate β-amyloid deposition can achieve accurate and reproducible assessments of [18F] FBB PET data. Also, a semi-quantitative analysis by SUVr cutoff classification was performed to obtain a significant result. Bullich et al[31] reported a good agreement between florbetaben PET quantification and histopathologic amyloid plaque density (92% sensitivity and 96% specificity) and visual read results by experts (percentage agreement = 94%∼97%). They emphasized the robustness of visual analysis performed by expert readers, as well as the additional contribution that optimized relative FBB uptake quantification may have for the detection of β-amyloid plaques.

Our study had some limitations. First, it was a retrospective observational study and may have selection bias. Our findings require external validation in larger cohorts. We also did not quantitatively assess the MR imaging–visible PVS burden in both the centrum semiovale and basal ganglia. Therefore, whether MR imaging–visible PVS in both the centrum semiovale and basal ganglia are consistent and good estimators of the whole-PVS load in the brain remains uncertain. Standardized, fully automated, and reliable whole-brain assessment techniques for PVS volume quantification are needed to generalize the results of our study.

CONCLUSIONS

The findings of this study provide further supporting evidence that MR imaging–visible PVS-CS are a key imaging marker of amyloid pathology when assessed by amyloid PET scans in patients with ADCI. Our findings raise the possibility that MR imaging–visible PVS-CS in patients with ADCI are also a consequence of amyloid deposition in the cortical and vascular amyloid processes.

REFERENCES

1. Doubal FN, MacLullich AM, Ferguson KJ, et al. **Enlarged perivascular spaces on MRI are a feature of cerebral small vessel disease.** *Stroke* 2010;41:450–54 CrossRef Medline
2. Brown R, Benveniste H, Black SE, et al. **Understanding the role of the perivascular space in cerebral small vessel disease.** *Cardiovasc Res* 2018;114:1462–73 CrossRef Medline
3. Zhu YC, Tzourio C, Soumare A, et al. **Severity of dilated Virchow-Robin spaces is associated with age, blood pressure, and MRI markers of small vessel disease: a population-based study.** *Stroke* 2010;41:2483–90 CrossRef Medline
4. Weller RO, Hawkes CA, Kalaria RN, et al. **White matter changes in dementia: role of impaired drainage of interstitial fluid.** *Brain Pathol* 2015;25:63–78 CrossRef Medline
5. Wardlaw JM, Benveniste H, Nedergaard M, et al. Colleagues from the Fondation Leducq Transatlantic Network of Excellence on the Role of the Perivascular Space in Cerebral Small Vessel Disease. **Perivascular spaces in the brain: anatomy, physiology and pathology.** *Nat Rev Neurol* 2020;16:137–53 CrossRef Medline
6. Park YW, Shin NY, Chung SJ, et al. **Magnetic resonance imaging–visible perivascular spaces in basal ganglia predict cognitive decline in Parkinson's disease.** *Mov Disord* 2019;34:1672–79 CrossRef Medline
7. Banerjee G, Kim HJ, Fox Z, et al. **MRI–visible perivascular space location is associated with Alzheimer's disease independently of amyloid burden.** *Brain* 2017;140:1107–16 CrossRef Medline
8. Smeijer D, Ikram MK, Hilal S. **Enlarged perivascular spaces and dementia: a systematic review.** *J Alzheimers Dis* 2019;72:247–56 CrossRef Medline
9. Inglese M, Bomsztyk E, Gonen O, et al. **Dilated perivascular spaces: hallmarks of mild traumatic brain injury.** *AJNR Am J Neuroradiol* 2005;26:719–24 Medline
10. Martinez-Ramirez S, Pontes-Neto OM, Dumas AP, et al. **Topography of dilated perivascular spaces in subjects from a memory clinic cohort.** *Neurology* 2013;80:1551–56 CrossRef Medline
11. Charidimou A, Meegahage R, Fox Z, et al. **Enlarged perivascular spaces as a marker of underlying arteriopathy in intracerebral haemorrhage: a multicentre MRI cohort study.** *J Neurol Neurosurg Psychiatry* 2013;84:624–29 CrossRef Medline
12. Charidimou A, Boulouis G, Pasi M, et al. **MRI–visible perivascular spaces in cerebral amyloid angiopathy and hypertensive arteriopathy.** *Neurology* 2017;88:1157–64 CrossRef Medline
13. van Veluw SJ, Biessels GJ, Bouvy WH, et al. **Cerebral amyloid angiopathy severity is linked to dilation of juxtacortical perivascular spaces.** *J Cereb Blood Flow Metab* 2016;36:576–80 CrossRef Medline
14. Raposo N, Planton M, Payoux P, et al. **Enlarged perivascular spaces and florbetapir uptake in patients with intracerebral hemorrhage.** *Eur J Nucl Med Mol Imaging* 2019;46:2339–47 CrossRef Medline
15. Martinez-Ramirez S, van Rooden S, Charidimou A, et al. **Perivascular spaces volume in sporadic and hereditary (Dutch-Type) cerebral amyloid angiopathy.** *Stroke* 2018;49:1913–19 CrossRef Medline
16. Roher AE, Kuo YM, Esh C, et al. **Cortical and leptomeningeal cerebrovascular amyloid and white matter pathology in Alzheimer's disease.** *Mol Med* 2003;9:112–22 CrossRef Medline
17. Charidimou A, Hong YT, Jager HR, et al. **White matter perivascular spaces on magnetic resonance imaging: marker of cerebrovascular amyloid burden?** *Stroke* 2015;46:1707–09 CrossRef Medline
18. Rowe CC, Ackerman U, Browne W, et al. **Imaging of amyloid beta in Alzheimer's disease with 18F-BAY94-9172, a novel PET tracer: proof of mechanism.** *Lancet Neurol* 2008;7:129–35 CrossRef Medline
19. Hawkes CA, Jayakody N, Johnston DA, et al. **Failure of perivascular drainage of beta-amyloid in cerebral amyloid angiopathy.** *Brain Pathol* 2014;24:396–403 CrossRef Medline
20. Ramirez J, Berezuk C, McNeely AA, et al. **Visible Virchow-Robin spaces on magnetic resonance imaging of Alzheimer's disease patients and normal elderly from the Sunnybrook Dementia Study.** *J Alzheimers Dis* 2014;43:415–24 CrossRef Medline
21. Marcus C, Mena E, Subramaniam RM. **Brain PET in the diagnosis of Alzheimer's disease.** *Clin Nucl Med* 2014;39:e413–22; quiz e23–26 CrossRef Medline
22. Murphy MP, LeVine H 3rd. **Alzheimer's disease and the amyloid-beta peptide.** *J Alzheimers Dis* 2010;19:311–23 CrossRef Medline
23. McKhann G, Drachman D, Folstein M, et al. **Clinical diagnosis of Alzheimer's disease: report of the NINCDS-ADRDA Work Group under the auspices of Department of Health and Human Services Task Force on Alzheimer's Disease.** *Neurology* 1984;34:939–44 CrossRef Medline
24. Petersen RC, Smith GE, Waring SC, et al. **Mild cognitive impairment: clinical characterization and outcome.** *Arch Neurol* 1999;56:303–08 CrossRef Medline
25. Ahn HJ, Chin J, Park A, et al. **Seoul Neuropsychological Screening Battery-dementia version (SNSB-D): a useful tool for assessing and monitoring cognitive impairments in dementia patients.** *J Korean Med Sci* 2010;25:1071–76 CrossRef Medline
26. Wardlaw JM, Smith EE, Biessels GJ, et al. STandards for ReportIng Vascular changes on nEuroimaging (STRIVE v1). **Neuroimaging standards for research into small vessel disease and its contribution to ageing and neurodegeneration.** *Lancet Neurol* 2013;12:822–38 CrossRef Medline
27. Maclullich AM, Wardlaw JM, Ferguson KJ, et al. **Enlarged perivascular spaces are associated with cognitive function in healthy elderly men.** *J Neurol Neurosurg Psychiatry* 2004;75:1519–23 CrossRef Medline
28. Fazekas F, Chawluk JB, Alavi A, et al. **MR signal abnormalities at 1.5 T in Alzheimer's dementia and normal aging.** *AJR Am J Roentgenol* 1987;149:351–56 CrossRef Medline
29. Barthel H, Gertz HJ, Dresel S, et al. **Cerebral amyloid-beta PET with florbetaben (18F) in patients with Alzheimer's disease and healthy controls: a multicentre phase 2 diagnostic study.** *Lancet Neurol* 2011;10:424–35 CrossRef Medline
30. Lopresti BJ, Klunk WE, Mathis CA, et al. **Simplified quantification of Pittsburgh Compound B amyloid imaging PET studies: a comparative analysis.** *J Nucl Med* 2005;46:1959–72 CrossRef Medline
31. Bullich S, Seibyl J, Catafau AM, et al. **Optimized classification of (18)F-Florbetaben PET scans as positive and negative using an SUVR quantitative approach and comparison to visual assessment.** *Neuroimage Clin* 2017;15:325–32 CrossRef Medline
32. Duara R, Loewenstein DA, Lizarraga G, et al. **Effect of age, ethnicity, sex, cognitive status and APOE genotype on amyloid load and the threshold for amyloid positivity.** *Neuroimage Clin* 2019;22:101800 CrossRef Medline

33. Francis F, Ballerini L, Wardlaw JM. **Perivascular spaces and their associations with risk factors, clinical disorders and neuroimaging features: a systematic review and meta-analysis.** *Int J Stroke* 2019;14:359–71 CrossRef Medline

34. Chen W, Song X, Zhang Y; Alzheimer's Disease Neuroimaging Initiative. **Assessment of the Virchow-Robin Spaces in Alzheimer disease, mild cognitive impairment, and normal aging, using high-field MR imaging.** *AJNR Am J Neuroradiol* 2011;32:1490–95 CrossRef Medline

35. Weller RO, Djuanda E, Yow HY, et al. **Lymphatic drainage of the brain and the pathophysiology of neurological disease.** *Acta Neuropathol* 2009;117:1–14 CrossRef Medline

36. Palmqvist S, Zetterberg H, Mattsson N, et al. Alzheimer's Disease Neuroimaging Initiative. **Detailed comparison of amyloid PET and CSF biomarkers for identifying early Alzheimer disease.** *Neurology* 2015;85:1240–49 CrossRef Medline

37. Buchhave P, Minthon L, Zetterberg H, et al. **Cerebrospinal fluid levels of beta-amyloid 1-42, but not of tau, are fully changed already 5 to 10 years before the onset of Alzheimer dementia.** *Arch Gen Psychiatry* 2012;69:98–106 CrossRef Medline

38. Hansson O, Zetterberg H, Buchhave P, et al. **Association between CSF biomarkers and incipient Alzheimer's disease in patients with mild cognitive impairment: a follow-up study.** *Lancet Neurol* 2006;5:228–34 CrossRef Medline

39. Hughes TM, Craft S, Lopez OL. **Review of 'the potential role of arterial stiffness in the pathogenesis of Alzheimer's disease.'** *Neurodegener Dis Manag* 2015;5:121–35 CrossRef Medline

40. Adams HH, Hilal S, Schwingenschuh P, et al. **A priori collaboration in population imaging: the Uniform Neuro-Imaging of Virchow-Robin Spaces Enlargement Consortium.** *Alzheimers Dement (Amst)* 2015;1:513–20 CrossRef Medline

41. Minoshima S, Drzezga AE, Barthel H, et al. **SNMMI Procedure Standard/EANM Practice Guideline for Amyloid PET Imaging of the Brain 1.0.** *J Nucl Med* 2016;57:1316–22 CrossRef Medline

42. Seibyl J, Barthel H, Stephens A, et al. **Reliability, reproducibility and efficacy of the 18F florbetaben β-amyloid PET scan visual assessment method as trained via a computer-based instructional tool.** *J Nucl Med* 2013;54(Suppl 2):300